Article

Not peer-reviewed version

Automated Aortic Quantification Based on Artificial Intelligence: Validation Using Contrast-Enhanced and Non-Contrast CT Scans from the Same Session

Jia-Sheng Hong , Yun-Hsuan Tzeng , Kuan-Ting Wu , Shih-Yu Huang , Ting Wei Wang , Guan-Yu Li , Chun-Yi Lin , Ho-Ren Liu , Hai-Neng Fu , Yung-Tsai Lee * , Wei-Hsian Yin * , Yu-Te Wu *

Posted Date: 26 February 2026

doi: 10.20944/preprints202602.1599.v1

Keywords: automated aortic quantification; artificial intelligence; computed tomography; aortic dilation; contrast-enhanced CT; non-contrast CT

Article

Automated Aortic Quantification Based on Artificial Intelligence: Validation Using Contrast-Enhanced and Non-Contrast CT Scans from the Same Session

Jia-Sheng Hong [1,†], Yun-Hsuan Tzeng [2,3,†], Kuan-Ting Wu [1,3], Shih-Yu Huang [1], Ting-Wei Wang[1,3], Guan-Yu Li [1], Chun-Yi Lin [1], Ho-Ren Liu [2], Hai-Neng Fu [4], Yung-Tsai Lee [5,6,*], Wei-Hsian Yin [3,4,*], Yu-Te Wu [1,7,8,*]

[1] Institute of Biophotonics, National Yang Ming Chiao Tung University, Taipei 112, Taiwan
[2] Health Management Center, Cheng Hsin General Hospital, Taipei 112, Taiwan
[3] School of Medicine, College of Medicine, National Yang Ming Chiao Tung University, Taipei 112, Taiwan
[4] Heart Center, Cheng Hsin General Hospital, Taipei 112, Taiwan
[5] Structural heart disease intervention, Heart Center, Cheng Hsin General Hospital, Taipei 112, Taiwan
[6] Department of Exercise and Healthy Science, National Taipei University of Nursing and Health Science, Taipei 112, Taiwan
[7] Brain Research Center, National Yang Ming Chiao Tung University, Taipei 112, Taiwan
[8] College Medical Device Innovation and Translation Center, National Yang Ming Chiao Tung University, Taipei 112, Taiwan
[†] These authors contributed equally to this work.
[*] Correspondence: andrewytlee.cvs@gmail.com (Y.-T.L.); yinwh88@gmail.com (W.-H.Y.); ytwu@nycu.edu.tw (Y.-T.W.)

Abstract

Artificial intelligence (AI) advancements have enabled automated aortic quantification in computed tomography (CT) imaging. We aimed to develop an AI method for quantifying the aorta in both contrast-enhanced and non-contrast CT scans, assisting early detection of aortic dilation. A total of 190 patient cases were analyzed, each having paired contrast-enhanced and non-contrast CT scans acquired in the same session, resulting in 380 scans. Our approach, based on open-source tools, demonstrated strong agreement with manual annotations, particularly in the ascending aorta. For contrast-enhanced CT, the AI achieved a correlation coefficient of 0.987 and intraclass correlation coefficient (ICC) of 0.986; for non-contrast CT, both were 0.945. Compared with clinical records, the sensitivity of AI detection was 97% for contrast-enhanced CT and 94% for non-contrast CT. This AI-based approach offers highly sensitive, automated aortic quantification across contrast conditions, supporting physicians in early identification of aortic abnormalities.

Keywords: automated aortic quantification; artificial intelligence; computed tomography; aortic dilation; contrast-enhanced CT; non-contrast CT

1. Introduction

As the primary artery, the aorta is pivotal in transporting oxygen-rich blood from the heart to the rest of the body, ensuring body organs receive the necessary oxygen for survival[1]. Its structure is vital for the integrity of this major blood vessel, with issues such as aneurysms and dissections posing significant life-threatening risks[2,3]. Aortic dilation is a crucial precursor to the aortic aneurysm, dissection, or in patients with aortic valve disease, requiring treatment intervention once surpassing certain thresholds[4,5]. The prevalence of aortic dilation ranges from 1.4% to 23%, varying across different study populations[6–8]. Aortic dilation is related to ageing and existing cardiovascular diseases or abnormalities, leading to an elevated risk of subsequent aortic disease[9].

 doi:10.20944/preprints202602.1599.v1

Advanced diagnostic techniques, such as echocardiography, MRI, and CT, enable early detection of aortic anomalies, ensuring timely treatment[10,11]. Following the guidelines, early surgical or pharmacological interventions have significantly enhanced patient prognosis, reducing the incidence of catastrophic outcomes[4,5]. Early detection and monitoring of aortic diseases can improve patient outcomes and minimize societal costs[12]. Non-contrast CT scans, such as those performed in lung cancer screening[13] as part of health screening programs, often include aortic imaging, offering an opportunity for early detection of aortic abnormalities. Maximizing the utility of any CT examination can significantly contribute to the early detection of diseases.

Artificial Intelligence (AI) techniques have rapidly advanced, enabling numerous automated analyses in medical imaging regarding cardiovascular imaging to become feasible[14]. In clinical AI applications, the variance in imaging techniques can pose challenges[15]. With its quantitative Hounsfield Units (HU), CT imaging is suitable for clinical AI applications. TotalSegmentator[16], introduced in early 2022, is a powerful AI model capable of segmenting various organs in CT images, advancing AI applications in CT imaging, including automated aortic segmentation[17–26]. While TotalSegmentator can automatically segment various tissues and organs in CT, a detailed and validated process for aortic quantification remains lacking. Should a method for quantifying the aorta be developed based on it and undergo proper validation, it would greatly benefit clinical diagnosis and monitoring.

Our research aims to develop and validate a fully automated aortic quantification process using TotalSegmentator as the core model. The workflow integrates automated processes and validates performance using paired CT images (contrast-enhanced and non-contrast) from the same patient within the same imaging session, ensuring clinical applicability.

2. Materials and Methods

2.1. Study Population

This study was a retrospective compilation of routine clinical imaging, receiving approval from the Institutional Review Board (IRB) of Cheng Hsin General Hospital (Approval No. [980] 111A-58). The IRB waived informed consent as all data were de-identified before analysis to ensure privacy, with no patient contact or intervention involved. All methods were performed in accordance with relevant guidelines and regulations, including those outlined by the Declaration of Helsinki and the IRB of Cheng Hsin General Hospital. A retrieval of 314 cases from the hospital's database was conducted between October 2021 and May 2023. Figure 1 depicts the patient selection waterfall diagram. Within this cohort of 314 cases, 29 exhibited pronounced aortic dissections with discernible true and false lumens. These instances were excluded from our study due to the challenge of distinguishing such cases in CT without contrast. Furthermore, 95 cases were excluded as they only had contrast-enhanced CTs, which did not meet our inclusion criteria. Consequently, 190 cases (380 scans) were incorporated into the study, with an age range between 42-94 (median of 74) and a gender ratio of 98:92 (male to female). Of these, we conducted manual aortic annotations on 134 cases (Test Set 1), while the remaining 56 cases did not receive such annotations (Test Set 2). All 190 cases came with clinical records from physicians, who, within their clinical practice, only proceeded with measurements in the presence of an apparent arterial dilation.

 doi:10.20944/preprints202602.1599.v1

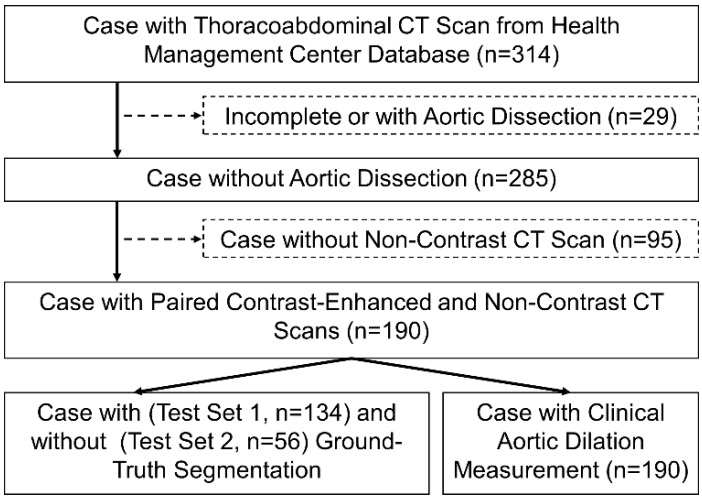

Figure 1. Patient selection flowchart. The flowchart demonstrates the stepwise representation of the inclusion and exclusion cases from the database for the study.

2.2. CT Imaging Protocol

The CT images were acquired using a dual-source 128-slice multidetector CT scanner (Somatom Definition FLASH, Siemens Healthineers, Erlangen, Germany). Two distinct imaging protocols were implemented. For contrast-enhanced scans, a slice thickness of 1 mm was selected, whilst non-contrast scans were conducted with a 3 mm slice thickness. All scans were performed at a voltage of 120 kVp with automated tube current modulation (CARE Dose4D, Siemens Healthineers). Additionally, pixel spacing for both protocols was the same at 0.65 mm, ensuring consistent spatial resolution across images. During imaging, patients were instructed to fully inhale, hold their breath, and remain still until advised to breathe normally again.

2.3. Ground-Truth Segmentation

We used the open-source medical image analysis platform 3D Slicer (https://slicer.org/) for manual semi-automated aorta annotation on contrast-enhanced CT images, utilizing the SegmentEditorExtraEffects and SlicerVMTK extensions. The watershed algorithm in the former segmented the aorta based on local histograms, while the Extract Centerline tool automatically detected inlets and outlets to extract the vessel's centerline. After initial segmentation, inaccurately segmented sections were corrected in 3D space, and the central line of the aorta was calculated. The aorta was then divided into the ascending aorta, aortic arch, and descending aorta based on the brachiocephalic trunk and left subclavian artery positions[27]. Annotations were performed by medical students and verified by experienced medical professionals.

2.4. Automated Aorta Quantification Workflow

Our automated aortic quantification process involved several steps (Figure 2). First, TotalSegmentator segmented tissues and organs in the CT images. The aorta was then extracted, and inlet and outlet points were automatically detected. If multiple points were identified, the two farthest apart were selected. Next, the vascular centerline was computed, straightened, and resampled to a uniform voxel size of 1 mm^3. Finally, the aorta's maximal diameter and cross-sectional area were calculated for each segment using the resampled images.

 doi:10.20944/preprints202602.1599.v1

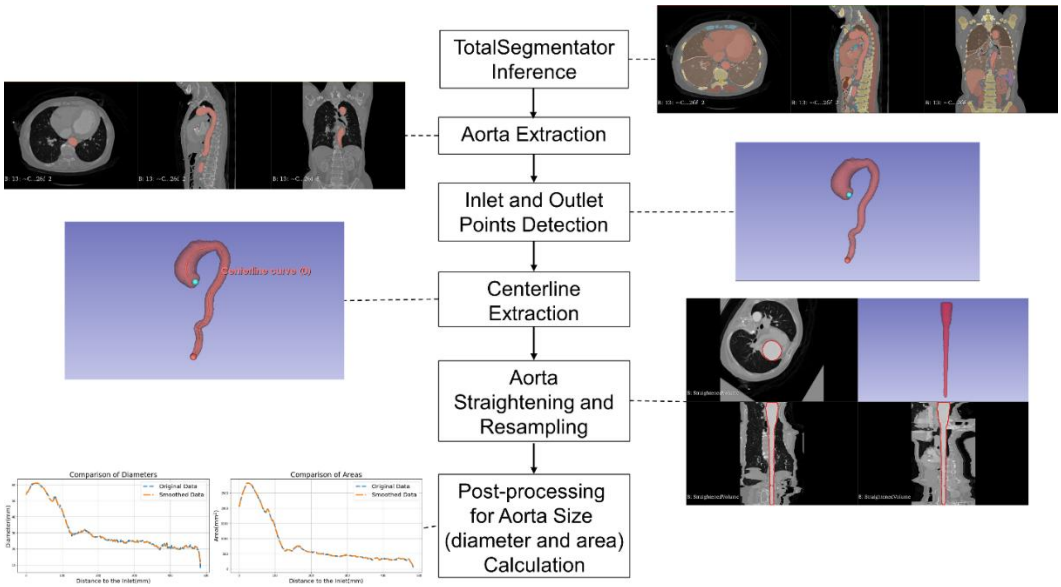

Figure 2. Automated aortic quantification AI process. Comprising six key steps, including TotalSegmentator inference, aortic extraction, inlet and outlet detection, vascular centreline extraction, aortic straightening and resampling, followed by post-processing of aortic dimension calculations.

We define segment levels based on the labelled positions, employing these distinct segments for subsequent AI results assessment. Additionally, leveraging the NumPy package (version 1.22.3), we automate the calculation of the maximum diameter and area size of cross-sections (Figure 3). A smoothing process was applied for the sequence of diameter and area values obtained using the Savitzky-Golay filter from the SciPy package (version 1.10.0), with a window length of 11 and a polynomial order of 2.

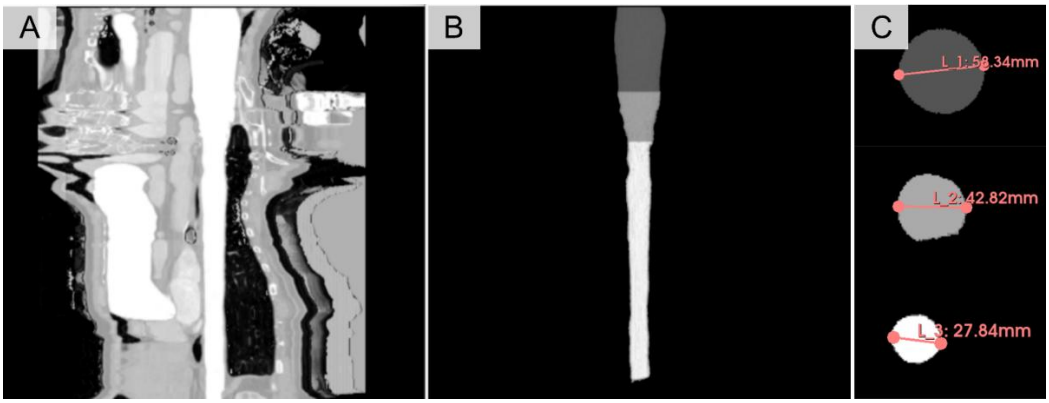

Figure 3. Schematic of aortic quantification. (A) Image of the aorta after straightening. (B) Label of the straightened aorta. (C) Schematic illustration of the area and maximum diameter of different aorta segments.

We developed an in-house 3D Slicer module, DeepAorta, integrating features from multiple extensions: TotalSegmentator (dcfa71b), SlicerVMTK (144582e), and Sandbox (94e2df0). The Extract Centerline tool in SlicerVMTK enabled automatic detection of the aorta's inlet and outlet points and centerline calculation, while the Sandbox Curved Planar Reformat extension facilitated vessel straightening and resampling based on the centerline. The software was deployed on 3D Slicer version 5.7.0, operating on a Windows 11 system. The primary hardware utilized was a CPU i9-13900K, with 64GB RAM, and a GPU NVIDIA GeForce RTX 4090 with 24GB VRAM.

2.5. Assessment of Measurements and Statistical Analysis

As previously mentioned, contrast-enhanced CT served as the gold standard for segmentation. We then compared the outcomes of AI-driven automatic quantification on contrast-enhanced and non-contrast CTs. Overlap-based metrics, such as the Dice similarity coefficient and the Intersection

 doi:10.20944/preprints202602.1599.v1

over Union (IoU), were evaluated alongside boundary-distance-based metrics, including the 95% Hausdorff distance and the average symmetric surface distance[28].

Furthermore, we evaluated the correlation and consistency for size measurements across the datasets. Our analysis employed the Pearson and intraclass correlation coefficients (ICC). This involves statistical analysis of aortic dimensions, including the diameter and area. Lastly, our study utilized Receiver Operating Characteristic (ROC) analysis between records in routine clinical procedures and AI quantification in identifying potential aortic dilation. Specific dilation thresholds were set for different regions[29]: 40mm for the ascending aorta, 35mm for the aortic arch, and 30mm for the descending aorta.

3. Results

3.1. Aortic Quantification Measurements

Table 1 presents the quantified results of aortic dimensions using GT, AI inference on CT with contrast and without contrast, divided into different segments: the entire aorta, ascending aorta, aortic arch, and descending aorta. The data encompassed maximum, mean, and median diameters/areas for the whole aorta, ascending aorta, aortic arch, and descending aorta.

Under the GT analysis, the whole aorta's maximum diameter was 38.28±5.42 mm, with the mean and median diameters at 27.17±3.17 mm and 25.31±3.14 mm, respectively. The maximum area recorded was 1047.94±350.20 mm², with mean and median areas at 554.99±136.80 mm² and 461.40±112.76 mm². An increase in aortic dimensions was observed utilizing AI inference on CT with contrast. The whole aorta's maximum diameter increased to 40.62±5.29 mm, and the maximum area to 1212.65±357.18 mm². Similar increments were noted across the ascending, arch, and descending segments. AI inference on CT without contrast further escalated the dimensions, where the whole aorta's maximum diameter reached 42.29±5.32 mm, and the maximum area was 1289.10±342.76 mm².

Table 1. Aortic dimensions for ground-truth segmentation and AI inference on CT with and without contrast.

Group / Segment	Diameter_{max}	Diameter_{mean}	Diameter_{median}	Area_{max}	Area_{mean}	Area_{median}
Ground Truth (GT)						
Whole Aorta	38.28 ± 5.42	27.17 ± 3.17	25.31 ± 3.14	1047.94 ± 350.20	554.99 ± 136.80	461.40 ± 112.76
Ascending	37.96 ± 5.47	34.45 ± 4.93	35.09 ± 5.18	1045.99 ± 351.13	881.44 ± 281.00	918.89 ± 291.88
Arch	36.07 ± 4.94	30.93 ± 3.60	30.45 ± 3.59	880.52 ± 243.10	666.80 ± 159.30	646.44 ± 158.83
Descending	28.34 ± 3.73	23.70 ± 2.82	23.18 ± 2.85	578.11 ± 150.22	409.09 ± 95.79	391.43 ± 95.50
CT_{AI} with Contrast						
Whole Aorta	40.62 ± 5.29	29.89 ± 3.01	28.07 ± 2.92	1212.65 ± 357.18	687.31 ± 145.57	587.28 ± 122.23
Ascending	40.35 ± 5.31	37.05 ± 4.77	37.65 ± 4.98	1210.50 ± 357.84	1041.52 ± 291.21	1074.78 ± 302.22
Arch	38.30 ± 4.74	32.67 ± 3.34	32.00 ± 3.30	1038.27 ± 253.26	786.01 ± 164.76	751.69 ± 163.93
Descending	31.00 ± 3.54	26.64 ± 2.72	26.19 ± 2.71	709.88 ± 163.62	533.40 ± 108.88	513.49 ± 107.23
CT_{AI} without Contrast						
Whole Aorta	42.29 ± 5.32	31.96 ± 2.97	30.40 ± 2.99	1289.10 ± 342.76	768.80 ± 144.65	675.77 ± 131.73
Ascending	41.98 ± 5.41	38.42 ± 4.76	39.23 ± 4.73	1286.14 ± 343.61	1098.55 ± 273.96	1142.13 ± 275.68

 doi:10.20944/preprints202602.1599.v1

Arch	39.20 ± 4.48	34.29 ± 3.72	33.90 ± 4.04	1081.55 ± 243.92	859.04 ± 188.75	840.79 ± 202.72
Descending	33.19 ± 3.55	29.06 ± 2.78	28.79 ± 2.81	798.20 ± 172.00	625.38 ± 119.07	611.88 ± 119.77

Note: GT denotes ground truth; CT_{AI} denotes AI inference in computed tomography images. All diameter measurements are expressed in millimeters (mm), and area measurements are in square millimeters (mm^2).

3.2. Segmentation Metrics

Table 2 delineates the segmentation metrics between GT and AI inference in CT images (CT_{AI}), both with and without contrast.

For GT versus CT_{AI} with contrast, the Dice coefficient ranged from 0.86±0.02 in the descending aorta to 0.91±0.02 in both the ascending aorta and aortic arch. The IoU scores were lowest for the descending aorta at 0.76±0.03 and highest for the ascending aorta at 0.84±0.03. The 95% Hausdorff distance was lowest for the ascending aorta at 2.27±0.53 mm and highest for the descending aorta at 2.63±0.56 mm. The average symmetric surface distance varied minimally, with the lowest observed in the aortic arch at 0.91±0.17 mm and the highest in the descending aorta at 1.44±0.17 mm.

In the comparison between GT and CT_{AI} without contrast, the Dice coefficients indicated lower conformity than CT_{AI} with contrast, ranging from 0.78±0.04 in the descending aorta to 0.87±0.03 in the ascending aorta. The IoU scores mirrored this trend, with the lowest score for the descending aorta at 0.65±0.05 and the highest for the ascending aorta at 0.77±0.05. The 95% Hausdorff distance increased, with the lowest distance in the aortic arch at 3.64±1.05 mm and the highest in the whole aorta at 4.24±0.72 mm. The average symmetric surface distance similarly increased, with the lowest in the aortic arch at 1.45±0.51 mm and the highest in the descending aorta at 2.37±0.35 mm.

Table 2. Segmentation metrics for ground-truth segmentation and AI inference on CT with and without contrast.

Segment	Dice	IoU	95% Hausdorff Distance (mm)	Average Symmetric Surface Distance (mm)
GT vs CT_{AI} with Contrast				
Whole Aorta	0.89±0.02	0.80±0.03	2.53±0.46	1.40±0.15
Ascending	0.91±0.02	0.84±0.03	2.27±0.53	1.15±0.16
Arch	0.91±0.02	0.83±0.04	2.30±0.55	0.91±0.17
Descending	0.86±0.02	0.76±0.03	2.63±0.56	1.44±0.17
GT vs CT_{AI} without Contrast				
Whole Aorta	0.82±0.03	0.70±0.05	4.24±0.72	2.25±0.32
Ascending	0.87±0.03	0.77±0.05	3.95±1.14	1.76±0.40
Arch	0.85±0.05	0.74±0.07	3.64±1.05	1.45±0.51
Descending	0.78±0.04	0.65±0.05	4.15±0.68	2.37±0.35

Note: GT denotes ground truth; CT_{AI} denotes AI inference in computed tomography images.

3.3. Correlation and Consistency Analysis

Figure 4 and Figure 5 depict the correlation coefficients and ICCs for the maximum diameter, illustrating the comparison between GT and CT_{AI}. (Please refer to Tables S1 and S2 for comprehensive values.)

In CT_{AI} with contrast, there was a high degree of similarity to the GT across all metrics. The correlation coefficient for the maximum diameter of ascending aorta was 0.987 (95% CI: 0.98-0.99). A similar pattern in ICCs, consistently near 1, indicated high reliability in measurements between GT and CT_{AI} with contrast.

The analysis of CT_{AI} without contrast revealed a decline in correlation coefficients and ICCs. The correlation coefficient for the maximum diameter of ascending aorta decreased to 0.945 (95% CI: 0.92-0.96), with a similarly reduced ICC. This trend was accentuated in the aortic arch, where the lowest ICCs were observed. This segment demonstrated the most variation, with correlation coefficients for

 doi:10.20944/preprints202602.1599.v1

median diameter dropping as low as 0.678 and ICCs reflecting this reduced agreement (Table 3 and Table 4). The descending aorta, while showing higher overall agreement than the arch in the CT_{AI} without contrast, presented a reduction in correlation coefficients and ICCs compared to the CT_{AI} with contrast.

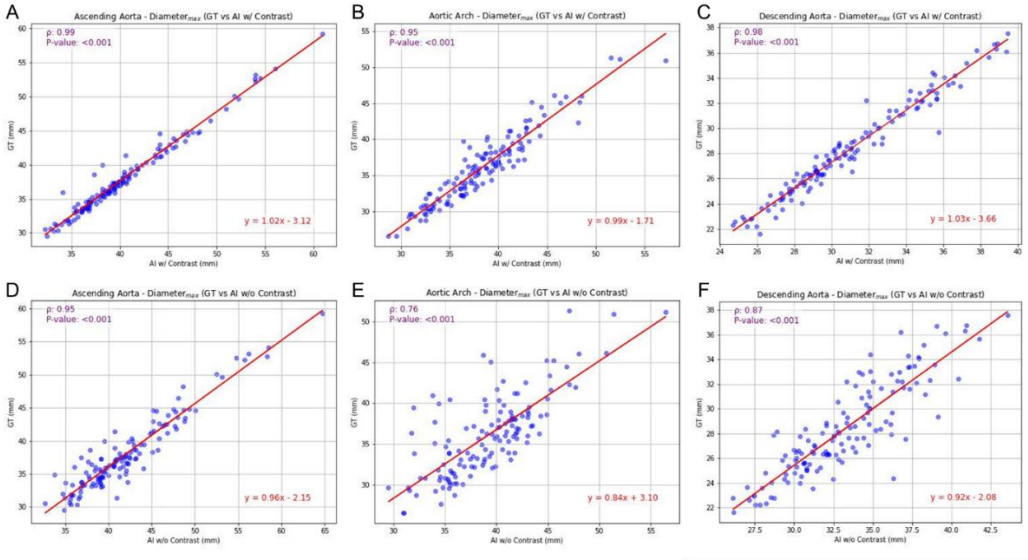

Figure 4. Scatter plot with correlation analysis for maximum diameter. GT versus CT_{AI} with contrast for (A) ascending aorta, (B) aortic arch, and (C) descending aorta. GT versus CT_{AI} without contrast for (D) ascending aorta, (E) aortic arch and (F) descending aorta.

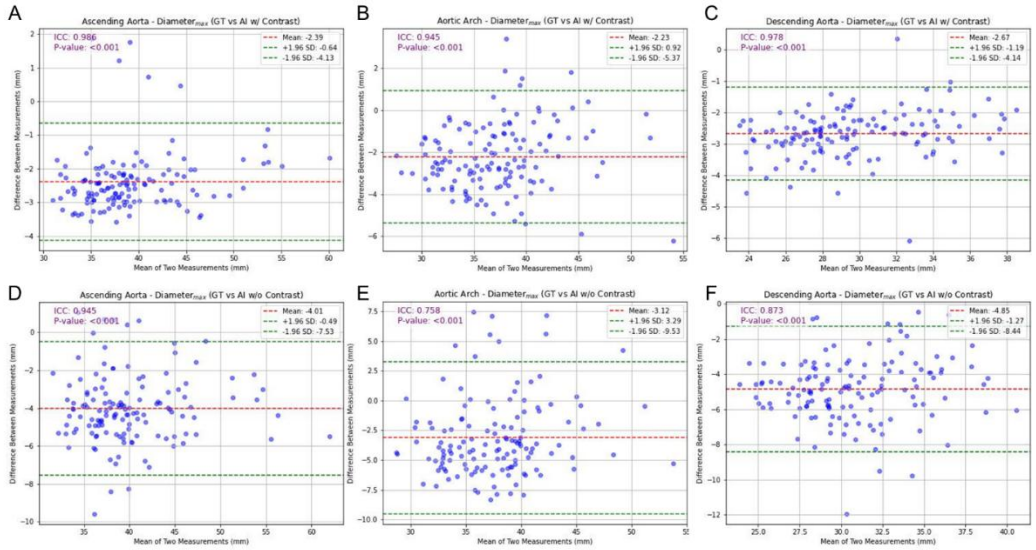

Figure 5. Bland-Altman plot with consistency analysis for maximum diameter. GT versus CT_{AI} with contrast for (A) ascending aorta, (B) aortic arch, and (C) descending aorta. GT versus CT_{AI} without contrast for (D) ascending aorta, (E) aortic arch, and (F) descending aorta.

Table 3. Correlation coefficients for aortic dimensions between ground truth and AI inference.

Segment	$Diameter_{max}$	$Diameter_{mean}$	$Diameter_{median}$	$Area_{max}$	$Area_{mean}$	$Area_{median}$
GT vs CT_{AI} with Contrast						
Ascending	0.987* [0.98-0.99]	0.998* [0.99-1.00]	0.998* [0.99-1.00]	0.997* [0.99-1.00]	0.997* [0.99-1.00]	0.997* [0.99-1.00]

 doi:10.20944/preprints202602.1599.v1

Arch	0.946* [0.92-0.96]		0.976* [0.97-0.98]		0.962* [0.95-0.97]		0.989* [0.98-0.99]	0.982* [0.97-0.99]	0.979* [0.97-0.99]
Descending	0.980* [0.97-0.99]		0.993* [0.99-0.99]		0.989* [0.99-0.99]		0.983* [0.98-0.99]	0.986* [0.98-0.99]	0.987* [0.98-0.99]
GT vs CT$_{AI}$ without Contrast									
Ascending	0.945* [0.92-0.96]		0.959* [0.94-0.97]		0.972* [0.96-0.98]		0.980* [0.97-0.99]	0.962* [0.95-0.97]	0.968* [0.96-0.98]
Arch	0.762* [0.68-0.82]		0.746* [0.66-0.81]		0.678* [0.57-0.76]		0.813* [0.75-0.86]	0.722* [0.63-0.79]	0.642* [0.53-0.73]
Descending	0.874* [0.83-0.91]		0.947* [0.93-0.96]		0.929* [0.90-0.95]		0.890* [0.85-0.92]	0.950* [0.93-0.96]	0.942* [0.92-0.96]

Note: GT, ground truth; CT$_{AI}$, AI inference in computed tomography images. * $p < 0.001$.

Table 4. Intraclass correlation coefficients for aortic dimensions between ground truth and AI inference.

Segment	Diameter$_{max}$	Diameter$_{mean}$	Diameter$_{median}$	Area$_{max}$	Area$_{mean}$	Area$_{median}$
GT vs CT$_{AI}$ with Contrast						
Ascending	0.986* [0.98-0.99]	0.997* [0.99-1.00]	0.997* [0.99-1.00]	0.997* [0.99-1.00]	0.996* [0.99-1.00]	0.996* [0.99-1.00]
Arch	0.945* [0.92-0.96]	0.973* [0.96-0.98]	0.958* [0.94-0.97]	0.988* [0.98-0.99]	0.982* [0.97-0.99]	0.979* [0.97-0.98]
Descending	0.978* [0.97-0.98]	0.992* [0.99-0.99]	0.988* [0.98-0.99]	0.980* [0.97-0.99]	0.978* [0.97-0.98]	0.981* [0.97-0.99]
GT vs CT$_{AI}$ without Contrast						
Ascending	0.945* [0.92-0.96]	0.958* [0.94-0.97]	0.968* [0.96-0.98]	0.979* [0.97-0.99]	0.962* [0.95-0.97]	0.967* [0.95-0.98]
Arch	0.758* [0.68-0.82]	0.746* [0.66-0.81]	0.673* [0.57-0.76]	0.813* [0.75-0.86]	0.711* [0.62-0.79]	0.623* [0.51-0.72]
Descending	0.873* [0.83-0.91]	0.947* [0.93-0.96]	0.929* [0.90-0.95]	0.882* [0.84-0.91]	0.927* [0.90-0.95]	0.918* [0.89-0.94]

Note: GT, ground truth; CT$_{AI}$, AI inference in computed tomography images. * $p < 0.001$. .

3.4. Receiver Operating Characteristic Analysis

In the ROC analysis (Figure 6), we compared the efficacy of physicians' routine clinical records and automated quantification in detecting aortic dilatation. Test Set 1 included 134 cases with GT segmentation, and Test Set 2 contained 56 cases lacking GT. These 190 cases featured routine clinical records from physicians, who recorded dilation measurements in the ascending aorta noted during clinical routines. For Test Set 2, we used the CT$_{AI}$'s quantification results from contrast-enhanced CTs, adjusted via regression correction from Test Set 1, as GT measurements. We were comparing the efficacy of physicians and CT$_{AI}$ in detecting aorta dilation in images without the contrast agent.

 doi:10.20944/preprints202602.1599.v1

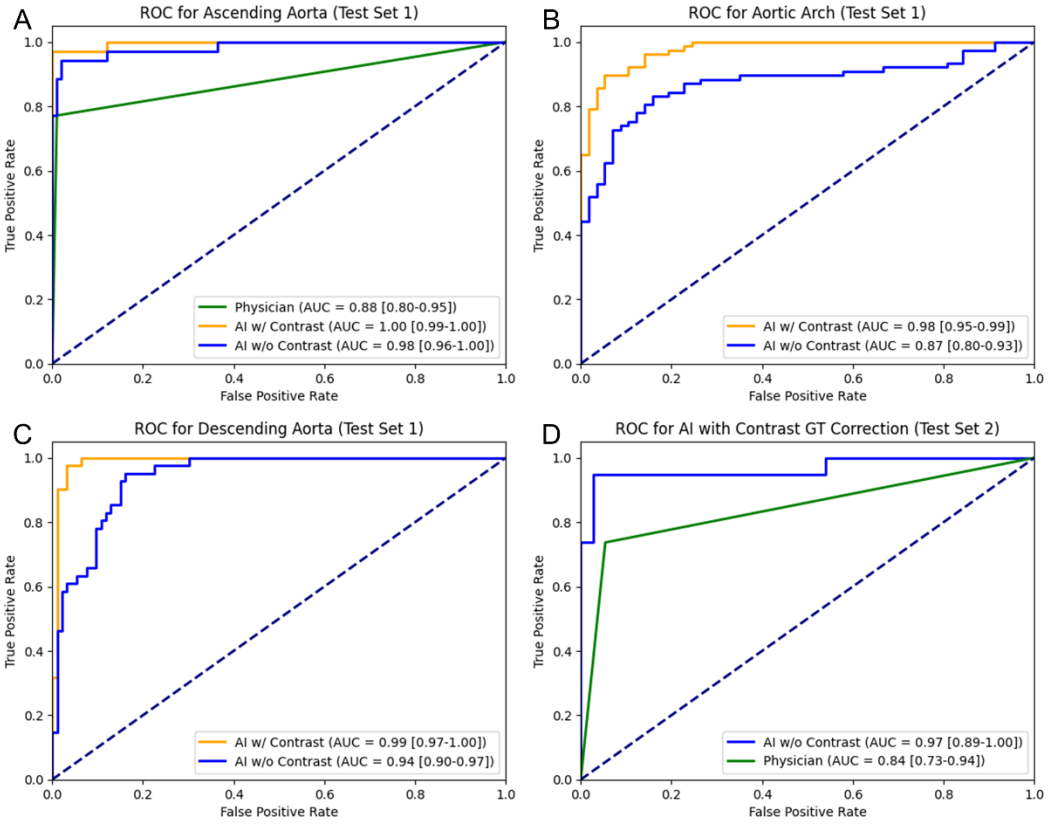

Figure 6. ROC analysis for comparing physicians and CTAI in assessing vascular dilation. (A) Ascending aorta, (B) aortic arch, and (C) descending aorta in Test Set 1. (D) Whole aorta in Test Set 2 (using quantification result from CTAI with contrast GT correction as GT).

For the ascending aorta in Test Set 1, the physician achieved an AUC of 0.88 [0.80-0.95], which was surpassed by the CTAI. CTAI with contrast reached the maximum AUC value of 0.997 [0.99-1.00], while that on CTAI without contrast also demonstrated superior accuracy with an AUC of 0.984 [0.96-1.00].

Considering the aortic arch in Test Set 1, there were no clinical records and CTAI with contrast had an AUC of 0.976 [0.95-0.99], whereas the performance of CTAI without contrast declined with an AUC of 0.874 [0.80-0.93]. For the descending aorta in Test Set 1, there were no clinical records, and the CTAI maintained a high level of diagnostic accuracy with contrast (AUC = 0.990 [0.97-1.00]) and without contrast (AUC = 0.942 [0.90-0.97]).

In Test Set 2, which lacked the GT segmentation and involved CTAI with contrast by GT correction as GT measurement for the aorta, CTAI performed robustly without contrast, achieving an AUC of 0.966 [0.89-1.00]. The physician's AUC in this set was 0.841 [0.73-0.94], lower than the CTAI without contrast. Table 5 documents the optimum sensitivity and specificity within the ROC analysis.

Table 5. Optimal metrics for receiver operating characteristic analysis.

Segment	Optimal Sensitivity	Optimal Specificity	AUC
Ascending Aorta			
Routine Records by Physicians	77%	99%	0.880 [0.80-0.95]
CTAI with Contrast	97%	100%	0.997 [0.99-1.00]
CTAI without Contrast	94%	98%	0.984 [0.96-1.00]
Aortic Arch			
CTAI with Contrast	90%	95%	0.976 [0.95-0.99]
CTAI without Contrast	83%	84%	0.874 [0.80-0.93]
Descending Aorta			
CTAI with Contrast	98%	97%	0.990 [0.97-1.00]
CTAI without Contrast	95%	84%	0.942 [0.90-0.97]

 doi:10.20944/preprints202602.1599.v1

Whole AortaCTAI with Contrast after GT Correction			
Routine Records by Physicians	74%	85%	0.841 [0.73-0.94]
CTAI without Contrast	95%	97%	0.966 [0.89-1.00]

Note: GT, ground truth; CT_{AI}, AI inference in computed tomography images.

4. Discussion

We developed a fully automated aortic quantification process using the open-source model and tools, demonstrating high effectiveness in detecting aortic dilation across CT imaging protocols, both with and without a contrast agent. The high degree of correlation and consistency in aortic quantification metrics (close to 1 for the maximum), alongside the impressive AUC scores in detecting vascular dilation (exceeding 0.9 across various segments and imaging protocols), underscore this fact. This reflects the model's potential to facilitate the early detection and longitudinal monitoring of aortic pathologies. This has the potential to redefine routine clinical imaging processes and, by promoting the early detection of aortic anomalies, to improve the prognoses for affected patients.

Our study observed distinct performance in evaluating aortic segments—ascending aorta, aortic arch, and descending aorta. Our semi-automatic method was based on contrast thresholds that defined the aortic lumen as GT. The AI's higher measurements stemmed from including the aortic wall, increasing thickness akin to the wall size[30]. The lack of wall contrast in non-contrast CT led to an even larger inclusion area. Nonetheless, the correlation and consistency results demonstrated the AI's exceptional capability in delineating the ascending aorta through contrast-enhanced and non-contrast CTs. Besides, AI performed better in contrast-enhanced CT than non-contrast CT, likely because the ground truth was based on contrast-enhanced CT, and the contrast agent highlighted vascular boundaries, improving AI segmentation and quantification. Irrespective of using a contrast agent, the AUC scores for all three aortic segments consistently exceeded 0.9 and surpassed clinical records, accentuating the AI's heightened sensitivity in detecting aortic dilation abnormalities. Nevertheless, despite a slight decline, the AI performance on non-contrast CT remains commendable. This suggests that AI could be utilized in scenarios where contrast agents are contraindicated, thereby widening the scope of non-invasive cardiovascular diagnostics. The capacity to discern aortic structure without contrast may have significant implications for patients with renal impairment or allergies to contrast media, offering a safer diagnostic alternative.

Clinical quantification of the aorta requires specialized software, and manual measurement is time-consuming and subject to certain errors[26]. If the imaging is not specifically conducted to examine the aorta, measurements are only undertaken when a noticeable dilation is observed upon reviewing the images. The AI application for automated aorta quantification saves time and keenly assists and alerts physicians to potential aortic abnormalities in patients. Recent research focusing on AI's application and validation for the automated quantification of the aorta has verified the exceptional accuracy of AI in aortic measurements, demonstrating its feasibility for clinical application[17–20,26]. Additionally, AI has proven adept at identifying aortic pathologies like aneurysms and dissections[22–25], with sensitivity and specificity on par with physicians, further highlighting its potential in clinical usage. By evaluating the AI performance across contrast-enhanced and non-contrast CTs in identical cases, our research has leveraged paired imaging to affirm AI's versatility in non-contrast CT settings, contributing to the discipline. Moreover, in contrast to other non-open source or commercial models, our approach is based entirely on the open-source model and tools, enhancing the reproducibility of our proposed methodologies.

Our study is subject to some limitations. Firstly, our validation was conducted on a single machine within a single center. However, the open-source core model we utilized, though not explicitly designed for aortic quantification, has been validated across multiple centers and machines for its accuracy and stability[16]. Secondly, the clinical records of aortic dilation measurements performed by various physicians were based on subjective assessments, with measurements taken only when aortic dilation was suspected. However, we addressed this issue by delineating the entire aorta and obtaining GT measurements through image processing. Theoretically, this approach should be more accurate and sensitive, a fact that was corroborated by our ROC analysis. Thirdly, our proposed process, centered around the TotalSegmentator as the core model, does not

 doi:10.20944/preprints202602.1599.v1

automatically segment the aorta into specific sections or infer results for different aortic landmarks as recommended[4,5]. Instead, our approach relies on statistical methods to identify the position of maximum values and calculate averages and medians from the entire aorta and different segments. Despite these constraints, we have validated the core model's accuracy in aorta quantification. Future developments based on this model and methodology may train more robust AI systems capable of automatically segmenting distinct aortic sections and detecting landmarks of interest.

5. Conclusions

We have developed an automated aortic quantification method anchored in the open-source model and tools. Our validation reveals that AI-powered automated aortic quantification enhances the clinical detection of abnormal aortic dilation via CT imaging, offering greater sensitivity than clinical routine records. This technology, which can be used in contrast-enhanced and non-contrast CT, affords physicians critical support in the early identification of unusual disease progression and the vigilant monitoring of patient aortic health.

Author Contributions: Conceptualization, J.-S.H.; Y.-H.T.; W.-H.Y.; methodology, J.-S.H.; Y.-H.T.; Y.-T.W.; software, J.-S.H.; K.-T.W.; C.-Y.L.; validation, T.-W.W.; H.-R.L.; H.-N.F.; formal analysis, J.-S.H.; investigation, J.-S.H.; K.-T.W.; S.-Y.H.; resources, G.-Y.L.; H.-R.L.; H.-N.F.; data curation, Y.-H.T.; H.-R.L.; Y.-T.L.; writing – original draft preparation, J.-S.H.; Y.-H.T.; writing – review and editing, J.-S.H.; Y.-H.T.; visualization, J.-S.H.; supervision, Y.-T.L.; W.-H.Y.; Y.-T.W.; project administration, Y.-T.L.; Y.-T.W.; funding acquisition, Y.-H.T.; Y.-T.W. All authors have read and agreed to the published version of the manuscript.

Funding: This research was funded by National Yang Ming Chiao Tung University and Cheng Hsin General Hospital, grant numbers CY11102, CY113-CY11201-01, CY113-CY11201-02, and CY113-CY11201-03.

Institutional Review Board Statement: The study was conducted in accordance with the Declaration of Helsinki and approved by the Institutional Review Board of Cheng Hsin General Hospital (Approval No. [980] 111A-58).

Informed Consent Statement: Patient consent was waived due to the retrospective nature of the study and the use of de-identified clinical data.

Data Availability Statement: The datasets generated and/or analyzed during the current study are not publicly available due to restrictions imposed by the approved protocol from the IRB of Cheng Hsin General Hospital (Approval No. [980] 111A-58), which did not include provisions for data sharing. All data were retrospectively collected and fully de-identified to protect patient privacy. Requests for access to the data can be made by contacting the corresponding author, subject to institutional approvals.

Acknowledgments: The authors would like to thank the Department of Radiology at Cheng Hsin General Hospital for their assistance in data retrieval. During the preparation of this manuscript, the authors used Grammarly (v1.2.162.1668) for English language editing and proofreading. The authors have reviewed and edited the output and take full responsibility for the content of this publication.

Conflicts of Interest: The authors declare no conflicts of interest.

References

1. Chirinos, J.A. Chapter 10 - Hemodynamic Role of the Aorta. In *Textbook of Arterial Stiffness and Pulsatile Hemodynamics in Health and Disease*; Chirinos, J.A., Ed.; Academic Press, 2022; pp. 155–168 ISBN 978-0-323-91391-1.
2. Koba, A.; Yamagishi, K.; Sairenchi, T.; Noda, H.; Irie, F.; Takizawa, N.; Tomizawa, T.; Iso, H.; Ota, H. Risk Factors for Mortality From Aortic Aneurysm and Dissection: Results From a 26-Year Follow-Up of a Community-Based Population. *J Am Heart Assoc* **2023**, *12*, e027045, doi:10.1161/JAHA.122.027045.
3. Fukui, T. Management of Acute Aortic Dissection and Thoracic Aortic Rupture. *Journal of Intensive Care* **2018**, *6*, 15, doi:10.1186/s40560-018-0287-7.
4. Authors/Task Force members; Erbel, R.; Aboyans, V.; Boileau, C.; Bossone, E.; Bartolomeo, R.D.; Eggebrecht, H.; Evangelista, A.; Falk, V.; Frank, H.; et al. 2014 ESC Guidelines on the Diagnosis and Treatment of Aortic Diseases: Document Covering Acute and Chronic Aortic Diseases of the Thoracic and

 doi:10.20944/preprints202602.1599.v1

Abdominal Aorta of the adultThe Task Force for the Diagnosis and Treatment of Aortic Diseases of the European Society of Cardiology (ESC). *European Heart Journal* **2014**, *35*, 2873–2926, doi:10.1093/eurheartj/ehu281.

5. Hiratzka, L.F.; Bakris, G.L.; Beckman, J.A.; Bersin, R.M.; Carr, V.F.; Casey, D.E.; Eagle, K.A.; Hermann, L.K.; Isselbacher, E.M.; Kazerooni, E.A.; et al. 2010 ACCF/AHA/AATS/ACR/ASA/SCA/SCAI/SIR/STS/SVM Guidelines for the Diagnosis and Management of Patients with Thoracic Aortic Disease: A Report of the American College of Cardiology Foundation/American Heart Association Task Force on Practice Guidelines, American Association for Thoracic Surgery, American College of Radiology, American Stroke Association, Society of Cardiovascular Anesthesiologists, Society for Cardiovascular Angiography and Interventions, Society of Interventional Radiology, Society of Thoracic Surgeons, and Society for Vascular Medicine. *Circulation* **2010**, *121*, e266-369, doi:10.1161/CIR.0b013e3181d4739e.
6. Babu, A.; Meng, Z.; Oji, O.; Bowker, T.; Xiao, H. How Common Is Aortic Dilatation? *European Heart Journal - Cardiovascular Imaging* **2021**, *22*, jeaa356.016, doi:10.1093/ehjci/jeaa356.016.
7. Meccanici, F.; de Bruijn, J.W.C.; Dommisse, J.S.; Takkenberg, J.J.M.; van den Bosch, A.E.; Roos-Hesselink, J.W. Prevalence and Development of Aortic Dilation and Dissection in Women with Turner Syndrome: A Systematic Review and Meta-Analysis. *Expert Review of Cardiovascular Therapy* **2023**, *21*, 133–144, doi:10.1080/14779072.2023.2172403.
8. Swahn, E.; Lekedal, H.; Engvall, J.; Nyström, F.H.; Jonasson, L. Prevalence and Determinants of Dilated Ascending Aorta in a Swedish Population: A Case–Control Study. *Eur Heart J Open* **2023**, *3*, oead085, doi:10.1093/ehjopen/oead085.
9. Niwa, K. Aortic Dilatation in Complex Congenital Heart Disease. *Cardiovasc Diagn Ther* **2018**, *8*, 725–738, doi:10.21037/cdt.2018.12.05.
10. Evangelista, A.; Flachskampf, F.A.; Erbel, R.; Antonini-Canterin, F.; Vlachopoulos, C.; Rocchi, G.; Sicari, R.; Nihoyannopoulos, P.; Zamorano, J.; European Association of Echocardiography; et al. Echocardiography in Aortic Diseases: EAE Recommendations for Clinical Practice. *Eur J Echocardiogr* **2010**, *11*, 645–658, doi:10.1093/ejechocard/jeq056.
11. Litmanovich, D.; Bankier, A.A.; Cantin, L.; Raptopoulos, V.; Boiselle, P.M. CT and MRI in Diseases of the Aorta. *American Journal of Roentgenology* **2009**, *193*, 928–940, doi:10.2214/AJR.08.2166.
12. Oude Wolcherink, M.J.; Behr, C.M.; Pouwels, X.G.L.V.; Doggen, C.J.M.; Koffijberg, H. Health Economic Research Assessing the Value of Early Detection of Cardiovascular Disease: A Systematic Review. *PharmacoEconomics* **2023**, *41*, 1183–1203, doi:10.1007/s40273-023-01287-2.
13. Baldwin, D.R.; Callister, M.E.J. An Update on CT Screening for Lung Cancer: The First Major Targeted Cancer Screening Programme. *Br J Radiol* **2020**, *93*, 20200636, doi:10.1259/bjr.20200636.
14. van Assen, M.; Razavi, A.C.; Whelton, S.P.; De Cecco, C.N. Artificial Intelligence in Cardiac Imaging: Where We Are and What We Want. *European Heart Journal* **2023**, *44*, 541–543, doi:10.1093/eurheartj/ehac700.
15. Wang, T.-W.; Shiao, Y.-C.; Hong, J.-S.; Lee, W.-K.; Hsu, M.-S.; Cheng, H.-M.; Yang, H.-C.; Lee, C.-C.; Pan, H.-C.; You, W.C.; et al. Artificial Intelligence Detection and Segmentation Models: A Systematic Review and Meta-Analysis of Brain Tumors in Magnetic Resonance Imaging. *Mayo Clinic Proceedings: Digital Health* **2024**, *2*, 75–91, doi:10.1016/j.mcpdig.2024.01.002.
16. Wasserthal, J.; Breit, H.-C.; Meyer, M.T.; Pradella, M.; Hinck, D.; Sauter, A.W.; Heye, T.; Boll, D.T.; Cyriac, J.; Yang, S.; et al. TotalSegmentator: Robust Segmentation of 104 Anatomic Structures in CT Images. *Radiology: Artificial Intelligence* **2023**, *5*, e230024, doi:10.1148/ryai.230024.
17. Artzner, C.; Bongers, M.N.; Kärgel, R.; Faby, S.; Hefferman, G.; Herrmann, J.; Nopper, S.L.; Perl, R.M.; Walter, S.S. Assessing the Accuracy of an Artificial Intelligence-Based Segmentation Algorithm for the Thoracic Aorta in Computed Tomography Applications. *Diagnostics (Basel)* **2022**, *12*, 1790, doi:10.3390/diagnostics12081790.
18. Portugal, M.F.C.; Pinheiro, L.L.; Lee, H.M.H.; Vieira, H.C.; Oliveira, L.L.; Valle, M.; Miyoshi, N.S.B.; Oliveira-Ciabati, L.; Baroni, R.; Szarf, G.; et al. Artificial Intelligence for Automated Thoracic Aorta Diameter Measurement Using Different Computed Tomography Protocols 2024.

 doi:10.20944/preprints202602.1599.v1

19. Katakol, S.; Bian, Z.; Lu, Y.; Spahlinger, G.; Hatt, C.R.; Burris, N.S. Fully Automated Aortic Measurements via CNN-Based Joint Segmentation and Localization. In Proceedings of the Medical Imaging 2023: Computer-Aided Diagnosis; SPIE, April 7 2023; Vol. 12465, pp. 246–250.
20. Graby, J.; Harris, M.; Jones, C.; Waring, H.; Lyen, S.; Hudson, B.J.; Rodrigues, J.C.L. Assessing the Role of an Artificial Intelligence Assessment Tool for Thoracic Aorta Diameter on Routine Chest CT. *British Journal of Radiology* **2023**, *96*, 20220853, doi:10.1259/bjr.20220853.
21. Hamelink, I. (Iris); de Heide, E. (Erik J.; Pelgrim, G.J. (Gert J.; Kwee, T.C. (Thomas); van Ooijen, P.M.A. (Peter); de Bock, G.H. (Truuske); Vliegenthart, R. (Rozemarijn) Validation of an AI-Based Algorithm for Measurement of the Thoracic Aortic Diameter in Low-Dose Chest CT. *European Journal of Radiology* **2023**, *167*, 111067, doi:10.1016/j.ejrad.2023.111067.
22. Bezerra de Carvalho Macruz, F.; Lu, C.; Strout, J.; Takigami, A.; Brooks, R.; Doyle, S.; Yun, M.; Buch, V.; Hedgire, S.; Ghoshhajra, B. Quantification of the Thoracic Aorta and Detection of Aneurysm at CT: Development and Validation of a Fully Automatic Methodology. *Radiology: Artificial Intelligence* **2022**, *4*, e210076, doi:10.1148/ryai.210076.
23. Mastrodicasa, D.; Codari, M.; Bäumler, K.; Sandfort, V.; Shen, J.; Mistelbauer, G.; Hahn, L.D.; Turner, V.L.; Desjardins, B.; Willemink, M.J.; et al. Artificial Intelligence Applications in Aortic Dissection Imaging. *Seminars in Roentgenology* **2022**, *57*, 357–363, doi:10.1053/j.ro.2022.07.001.
24. Sieren, M.M.; Widmann, C.; Weiss, N.; Moltz, J.H.; Link, F.; Wegner, F.; Stahlberg, E.; Horn, M.; Oecherting, T.H.; Goltz, J.P.; et al. Automated Segmentation and Quantification of the Healthy and Diseased Aorta in CT Angiographies Using a Dedicated Deep Learning Approach. *Eur Radiol* **2022**, *32*, 690–701, doi:10.1007/s00330-021-08130-2.
25. Hata, A.; Yanagawa, M.; Yamagata, K.; Suzuki, Y.; Kido, S.; Kawata, A.; Doi, S.; Yoshida, Y.; Miyata, T.; Tsubamoto, M.; et al. Deep Learning Algorithm for Detection of Aortic Dissection on Non-Contrast-Enhanced CT. *Eur Radiol* **2021**, *31*, 1151–1159, doi:10.1007/s00330-020-07213-w.
26. Pradella, M.; Weikert, T.; Sperl, J.I.; Kärgel, R.; Cyriac, J.; Achermann, R.; Sauter, A.W.; Bremerich, J.; Stieltjes, B.; Brantner, P.; et al. Fully Automated Guideline-Compliant Diameter Measurements of the Thoracic Aorta on ECG-Gated CT Angiography Using Deep Learning. *Quant Imaging Med Surg* **2021**, *11*, 4245–4257, doi:10.21037/qims-21-142.
27. Kelley, J.D.; Kerndt, C.C.; Ashurst, J.V. Anatomy, Thorax, Aortic Arch. In *StatPearls*; StatPearls Publishing: Treasure Island (FL), 2024.
28. Yeghiazaryan, V.; Voiculescu, I. Family of Boundary Overlap Metrics for the Evaluation of Medical Image Segmentation. *J Med Imaging (Bellingham)* **2018**, *5*, 015006, doi:10.1117/1.JMI.5.1.015006.
29. Obel, L.M.; Diederichsen, A.C.; Steffensen, F.H.; Frost, L.; Lambrechtsen, J.; Busk, M.; Urbonaviciene, G.; Egstrup, K.; Karon, M.; Rasmussen, L.M.; et al. Population-Based Risk Factors for Ascending, Arch, Descending, and Abdominal Aortic Dilations for 60-74-Year-Old Individuals. *J Am Coll Cardiol* **2021**, *78*, 201–211, doi:10.1016/j.jacc.2021.04.094.
30. Liu, C.-Y.; Chen, D.; Bluemke, D.A.; Wu, C.O.; Teixido-Tura, G.; Chugh, A.; Vasu, S.; Lima, J.A.C.; Hundley, W.G. Evolution of Aortic Wall Thickness and Stiffness with Atherosclerosis: Long-Term Follow up from the Multi-Ethnic Study of Atherosclerosis (MESA). *Hypertension* **2015**, *65*, 1015–1019, doi:10.1161/HYPERTENSIONAHA.114.05080.